Effects of bending and torsion rigidity on deformation and breakage of flexible fibers : a direct simulation study

Kabanemi, Kalonji K.; Hétu, Jean-François

Publisher's version / Version de l'éditeur:
https://doi.org/10.1063/1.3685832
The Journal of Chemical Physics, 136, 7, pp. 074903-074911, 2012-02-17

Effects of bending and torsion rigidity on deformation and breakage of flexible fibers: A direct simulation study

Kalonji K. Kabanemi [(a)] and Jean-François Hétu
Industrial Materials Institute (IMI), National Research Council of Canada (NRC)
75 de Mortagne, Boucherville, Québec, Canada, J4B 6Y4

[(a)] Author to whom correspondence should be addressed; electronic mail: kalonji.kabanemi@cnrc-nrc.gc.ca

Abstract

To understand the various mechanisms of fiber deformation of flexible fiber suspensions, we carry out a direct simulation study to analyze the effect of fiber rigidity on fiber motion in simple shear flow. Such a study may be used to investigate the critical parameters controlling the breakage of flexible fibers during processing. We model the fiber as a series of rigid spheres connected by stiff springs. The stretching, bending and torsional rigidities are determined by Young's modulus and shear modulus to realistically model the fiber rigidity. The model correctly predicts the orbit period of fiber rotation, $T\dot{\gamma}$, as well as the trend of critical flow strength, $\eta\dot{\gamma}/E$, versus fiber aspect ratio, r_p, at which breakage occurs in simple shear flow.

I. INTRODUCTION

The prediction of deformation of flexible fibers in any type of flow represents an important step in the understanding of how process conditions along with the flow field domain may induce fiber degradation. To investigate the various mechanisms of fiber breakage, and to improve the manufacturing procedure of long fiber reinforced systems, it is of interest to understand the dynamics of flowing flexible fiber suspensions. The present work contributes to this issue by constructing a fiber model that can be used for quantitative predictions of critical flow conditions required to break fibers of specific mechanical properties, and aspect ratios, in any type of flow and any flow domain.

Among the various models based on molecular approach to study the dynamics of rigid rodlike macromolecules, the most relevant is the one developed by Doi and Edwards [1]. For the shish-kebab model, the rod is regarded as made up of N beads placed along a straight line. The adequacy of the model for estimating the rotational friction constant of a rigid rodlike macromolecule has been demonstrated. As originally presented, the shish-kebab model of Doi and Edwards, deals only with rigid rodlike macromolecules. However, extension of the model to a class of macromolecules or fibers which are flexible is straightforward. Along these lines, Yamamoto and Matsuoka [2-5] proposed a method for simulating the dynamic behavior of rigid and flexible fibers in a flow field. Similar to the shish-kebab model, the fiber is regarded as made up of spheres that are lined up and bonded to each neighbor. Each pair of bonded spheres can stretch, bend, and twist, by changing their bond distance, bond angle, and torsion angle, respectively. Although Yamamoto and Matsuoka showed that the proposed model successfully reproduced the dynamic behavior of rigid and flexible fibers in a shear flow, we found that the numerical results were artificially enforced to match those of Jeffery's theory [6]. In fact, to ensure that the nonslip conditions between bonded spheres were not broken in their model, the angles of spheres were manually adjusted at each time step to satisfy the nonslip conditions. Without any adjustment of the angles of spheres, the model failed to predict the orbit period of fiber rotation. Since the bending deformation in that model was not correctly handled, such an adjustment was necessary to match results already published in the literature. Indeed, we did various numerical validations of the model without adjustment, and found that the period of fiber rotation was not constant, and depended on the initial orientation of the fiber. Furthermore, in the different studies of Yamamoto and Matsuoka, the twist deformation, which is rather difficult to handle, was only addressed superficially. Recently, Qi [7] developed a method for direct simulations of flexible filament suspensions in a non-zero Reynolds number flow. For fluid domain, simulations were based on a lattice Boltzmann equation, while for solid domain, a slender solid body was discretized into a chain of consecutive spherical segments contacting each other. A constraint force algorithm was proposed to warrant constant bonding distance between two neighboring segments and non-slip velocity conditions at the contacting points so that the flexible filament moves and rotates as a whole body. The fibre could be bent and twisted in the model. The method was tested by using a rigid particle method when the fibre stiffness is very large and by comparing the results with theoretical and experimental results. Ning and Melrose [8] presented a numerical method for simulating

the mechanical behavior of flexible fibers. The fiber was made up by a number of short cylinders and bonded to each neighbor. Bending deflection and twist movement occur respectively in the bending and torsion planes. The numerical model was applied to study rotation of rigid and flexible fibers in a shear flow. Ross and Klingenberg [9], and Skjetne et al. [10] employed a particle-level simulation method to study the dynamics of flowing suspensions of rigid and flexible fibers. Fibers were modeled as chains of prolate spheroids connected through ball and socket joints. By varying the resistance in the joints, both flexible and rigid fibers were modeled. Lindström and Uesaka [11] proposed a model for fibers suspended in a viscous fluid. Flexible fibers were modeled as chains of fiber segments. Quantitative predictions were made, and showed good agreement with experimental data. As far as fiber degradation is concerned, Salinas and Pittman [12] made an experimental study of fiber breakage in sheared suspensions, and derived two correlations that can be used to predict breaking conditions for fibers of known Young's modulus and ultimate tensile strength. Franzén et al. [13] reported measurements of fiber degradation in short fiber reinforced thermoplastics subjected to various compounding methods. In their study, it appeared difficult to relate the fiber length reduction to a single dominant mechanism. Nevertheless, they observed that the fiber concentration has only a limited effect on the final length distribution, while the buckling could be a key factor among the various possible causes of fibre degradation.

Taking advantage of these insights, we carry out a direct simulation study to analyze the effect of fiber rigidity on fiber motion in a simple shear flow. The fiber model is similar to that used by Doi and Edwards for the shish-kebab model and Yamamoto and Matsuoka. However, unlike Yamamoto and Matsuoka, in the present study the bending deformation made by two adjacent bonds defined by three adjacent spheres, is estimated by taking the vector products of bonds connected the spheres, while the three Euler angles are introduced to track the torsional deformation. As the bending and torsional motions are correctly handled, numerical adjustments of the angles of spheres at each time step, to artificially enforce the nonslip conditions between bonded spheres, like Yamamoto and Matsuoka, are no longer required. Such a study may be used to investigate the critical parameters controlling the breakage of flexible fibers during processing. The paper is organized as follows: We first present the fiber model and the simulation method. Next, we introduce the basic equations of motion of the fiber model. Then, we derive explicitly the hydrodynamic and non- hydrodynamic forces and torques exerted on spheres of the fiber model. In the subsequent section, we analyse the behavior of the underlying model in a simple shear flow, and perform quantitative comparisons with the experimental data provided by Trevelyan and Mason [14]. A final discussion on the various mechanisms for fiber breakage concludes the paper.

II. MODEL

We model the flexible fiber of contour length, L, as a series of $N = \frac{L}{2a}$ rigid spheres (beads) of diameter $2a$, connected successively, in three-dimensional space, by $N-1$ stiff springs (bonds) of equilibrium length, $2a$, as illustrated in Fig. 1. A similar model

has been first used by Doi and Edwards for the shish-kebab model to estimate the rotational friction constant of a rigid rod, and subsequently by Yamamoto and Matsuoka. Here, the instantaneous configuration of the flexible fiber of N rigid spheres, in three-dimensional space, is described by a set of sphere position vectors, $\{\boldsymbol{r}_i\}_{i=1,N}$, each of components $\boldsymbol{r}_i = (r_{i,x}, r_{i,y}, r_{i,z})$, measured from a fixed reference space frame $\{\boldsymbol{X}, \boldsymbol{Y}, \boldsymbol{Z}\}$, and three Euler angles, $(\phi_i, \theta_i, \psi_i)_{i=1,N}$, for each individual sphere, specifying the orientation of the ith sphere, for a given location of its center. These three Euler angles represent three composed rotations that move a fixed reference frame to a given referred frame. To specify the orientations of the spheres placed along the fiber, a set of local body coordinate unit vectors, $\{\boldsymbol{m}_i, \boldsymbol{n}_i, \boldsymbol{t}_i\}_{i=1,N-1}$, defining the local orthogonal coordinate frames is assigned to all paired spheres, $(i, i+1)_{i=1,N-1}$, i.e., to all bonds of the fiber model, such that the unit bond vector, $\boldsymbol{t}_i$, pointing to the center of the sphere $i+1$ from the center of the sphere i, is defined as

$$\boldsymbol{t}_i = \frac{\boldsymbol{r}_{i+1} - \boldsymbol{r}_i}{|\boldsymbol{r}_{i+1} - \boldsymbol{r}_i|}, \tag{1}$$

where, $|\boldsymbol{r}_{i+1} - \boldsymbol{r}_i|$, is the distance between the spheres i and $i+1$. The unit vectors, $\boldsymbol{m}_i$, and $\boldsymbol{n}_i$, are chosen in the plane perpendicular to $\boldsymbol{t}_i$. To compare the orientations of the fixed reference space coordinate system, $\{\boldsymbol{X}, \boldsymbol{Y}, \boldsymbol{Z}\}$, and the local body coordinate system, $\{\boldsymbol{m}_i, \boldsymbol{n}_i, \boldsymbol{t}_i\}$, attached to a pair of bonded spheres, $(i, i+1)$, the three Euler angles (ϕ, θ, ψ) are employed. If the reference space coordinate system is rotated through these three Euler angles, it will be brought into alignment with the body axes. This sequence of three rotations is illustrated in Fig. 2, where the x-convention of the Euler angles is used. Then, the three Euler angles (ϕ, θ, ψ) between the two frames can be obtained as follows

$$\phi = \arccos\left(-\frac{t_{i,x}}{\sqrt{1-t_{i,z}^2}}\right), \tag{2}$$

$$\theta = \arccos\left(t_{i,z}\right), \tag{3}$$

$$\psi = \arccos\left(\frac{n_{i,z}}{\sqrt{1-t_{i,z}^2}}\right). \tag{4}$$

The three Euler angles (ϕ, θ, ψ) are uniquely determined except for the singular cases that occur when θ approaches 0 or π. These cases must be handled specially. Before going any further and to avoid confusion at this stage, let us consider a pair of bonded spheres, $(i, i+1)$, positioned at $\boldsymbol{r}_i$ and $\boldsymbol{r}_{i+1}$, along the fiber. It is important to emphasize that the Euler angle, ψ, as expressed by Eq. (4) defines precisely the intrinsic or rigid angular displacements, ψ_i^R, and ψ_{i+1}^R, of the paired spheres $(i, i+1)$ around the unit bond

vector $\boldsymbol{t}_i$, as a result of their spatial locations, i.e., $\psi_i^R = \psi_{i+1}^R = \psi$. Furthermore, since the orientation of the local body axes changes along the fiber contour length, the Euler angles, (ϕ, θ, ψ), also vary at any point along the fiber.

Next we consider how to calculate the instantaneous rotation of the spheres of the fiber model. To this end, let $(\omega_{i,x}, \omega_{i,y}, \omega_{i,z})$ be the components of the angular velocity, $\boldsymbol{\omega}_i$, of the ith sphere relative to the fixed reference space coordinate system. It can be shown that these components may be expressed in terms of the Euler angles, in the fixed reference space frame, as

$$\boldsymbol{\omega}_i = \omega_{i,x}\boldsymbol{X} + \omega_{i,y}\boldsymbol{Y} + \omega_{i,z}\boldsymbol{Z} = \begin{bmatrix} \omega_{i,x} \\ \omega_{i,y} \\ \omega_{i,z} \end{bmatrix} = \begin{bmatrix} \dot{\theta}_i \cos\phi_i + \dot{\psi}_i \sin\theta_i \sin\phi_i \\ \dot{\theta}_i \sin\phi_i - \dot{\psi}_i \sin\theta_i \cos\phi_i \\ \dot{\phi}_i + \dot{\psi}_i \cos\theta_i \end{bmatrix}. \tag{5}$$

Inversion of this set of equations, gives the instantaneous rotation of the ith sphere with respect to the fixed reference space coordinate system in terms of the components of its angular velocity, $\boldsymbol{\omega}_i$, as

$$\begin{bmatrix} \dot{\phi}_i \\ \dot{\theta}_i \\ \dot{\psi}_i \end{bmatrix} = \begin{bmatrix} \omega_{i,z} - (\omega_{i,x}\sin\phi_i - \omega_{i,y}\cos\phi_i)\cos\theta_i / \sin\theta_i \\ \omega_{i,x}\cos\phi_i + \omega_{i,y}\sin\phi_i \\ (\omega_{i,x}\sin\phi_i - \omega_{i,y}\cos\phi_i)/\sin\theta_i \end{bmatrix}. \tag{6}$$

By using the standard Euler integration of Eq. (6), the explicit expression for the angular displacement of the ith sphere around the unit bond vector $\boldsymbol{t}_i$, or the torsional angle, ψ_i^n, at each time step can be written as

$$\psi_i^n = \psi_i^{n-1} + \psi_i^R + \Delta t\,(\omega_{i,x}^n \sin\phi_i^R - \omega_{i,y}^n \cos\phi_i^R)/\sin\theta_i^R. \tag{7}$$

It is apparent from Eq. (7), that the angular displacement, ψ_i^n, depends upon the angular velocity at current time, ω_i^n. This equation allows us to define, in a transparent manner, the link between the torsional angle of the sphere i at each stage of deformation and its angular velocity. Since the rotational motions of the spheres are considered explicitly, Eq. (7) will be useful in the calculation of the torsional restoring torque acting on each sphere of the fiber model.

We shall now summarize the basic equations of the fiber motion on which our subsequent analysis is based. The translational and rotational motion of each sphere, i, of the fiber, immersed in an incompressible fluid may be described by the equations of motion

$$m_i \frac{d\boldsymbol{u}_i}{dt} = \boldsymbol{F}_i^h + \boldsymbol{F}_i^{nh}, \tag{8}$$

$$I_i \frac{d\boldsymbol{\omega}_i}{dt} = \boldsymbol{M}_i^h + \boldsymbol{M}_i^{nh}, \tag{9}$$

where $\boldsymbol{u}_i = \frac{d\boldsymbol{r}_i}{dt}$ and $\boldsymbol{\omega}_i = \frac{d\boldsymbol{\theta}_i}{dt}$ are, respectively, the translational velocity and the angular velocity of the sphere i, $\boldsymbol{\theta}_i = (\theta_{i,x}, \theta_{i,y}, \theta_{i,z})$ is the angular position relative to the fixed reference space coordinate system, m_i and $I_i = 2m_i a_i^2 / 5$ are, respectively, the mass and the moment of inertia, $\boldsymbol{F}_i^h$ and $\boldsymbol{M}_i^h$ are, respectively, the force and the torque exerted by the fluid on sphere i, and $\boldsymbol{F}_i^{nh}$ and $\boldsymbol{M}_i^{nh}$ are, respectively, the total non-hydrodynamic force and torque on this sphere. In the linear regime considered here the velocities and the angular velocities of the spheres are related to the forces and torques exerted on them by the fluid, by a set of coupled linear equations of the form [15]

$$\boldsymbol{u}_i - \boldsymbol{u}_0(\boldsymbol{r}_i) = -\boldsymbol{H}_{ij}^{TT} \cdot \boldsymbol{F}_j^h - \boldsymbol{H}_{ij}^{TR} \cdot \boldsymbol{M}_j^h, \tag{10}$$

$$\boldsymbol{\omega}_i - \boldsymbol{\omega}_0(\boldsymbol{r}_i) = -\boldsymbol{H}_{ij}^{RT} \cdot \boldsymbol{F}_j^h - \boldsymbol{H}_{ij}^{RR} \cdot \boldsymbol{M}_j^h. \tag{11}$$

Here $\boldsymbol{u}_0(\boldsymbol{r}_i)$, and $\boldsymbol{\omega}_0(\boldsymbol{r}_i)$ are, respectively, the velocity and the vorticity of the fluid evaluated at the position of the sphere i, $\boldsymbol{H}_{ij}^{TT}$ is the translational mobility tensor, $\boldsymbol{H}_{ij}^{RR}$ the rotational mobility tensor, and the matrices $\boldsymbol{H}_{ij}^{TR}$ and $\boldsymbol{H}_{ij}^{RT}$ couple translational and rotational motion between spheres i and j. Note that $\boldsymbol{u}_i$, $\boldsymbol{\omega}_i$, $\boldsymbol{F}_i^h$ and $\boldsymbol{M}_i^h$ are vectors and therefore each component of the mobility tensors is a tensor. Explicit expressions for these mobility tensors have been presented by Mazur and Van Saarloss [15] up to order $\left|\boldsymbol{r}_i - \boldsymbol{r}_j\right|^{-7}$. The leading terms of each component of the mobility tensors for two-sphere interactions are

$$H_{ii,\alpha\beta}^{TT} = \frac{\delta_{\alpha\beta}}{\zeta_T}, \tag{12}$$

$$H_{ij,\alpha\beta}^{TT} = \frac{1}{8\pi\eta\left|\boldsymbol{r}_i - \boldsymbol{r}_j\right|}\left(\delta_{\alpha\beta} + \frac{(r_{i,\alpha} - r_{j,\alpha})(r_{i,\beta} - r_{j,\beta})}{\left|\boldsymbol{r}_i - \boldsymbol{r}_j\right|^2}\right), \tag{13}$$

$$H_{ii,\alpha\beta}^{RR} = \frac{\delta_{\alpha\beta}}{\zeta_R}, \tag{14}$$

$$H_{ij,\alpha\beta}^{RR} = \frac{1}{16\pi\eta\left|\boldsymbol{r}_i - \boldsymbol{r}_j\right|^3}\left(3\frac{\left(r_{i,\alpha} - r_{j,\alpha}\right)\left(r_{i,\beta} - r_{j,\beta}\right)}{\left|\boldsymbol{r}_i - \boldsymbol{r}_j\right|^2} - \delta_{\alpha\beta}\right), \tag{15}$$

$$H_{ii,\alpha\beta}^{TR} = H_{ii,\alpha\beta}^{RT} = 0, \tag{16}$$

$$H_{ij,\alpha\beta}^{RT} = -H_{ji,\alpha\beta}^{TR} = -\frac{1}{8\pi\eta\left|\boldsymbol{r}_i - \boldsymbol{r}_j\right|^2}\varepsilon_{\alpha\beta\gamma}\frac{\left(r_{i,\gamma} - r_{j,\gamma}\right)}{\left|\boldsymbol{r}_i - \boldsymbol{r}_j\right|}, \tag{17}$$

where i and j label the individual spheres, while $\alpha,\beta,\gamma = x,y,z$ label the Cartesian coordinates, $\varepsilon_{\alpha\beta\gamma}$ is the permutation symbol, $\zeta_T = 6\pi\eta a$ and $\zeta_R = 8\pi\eta a^3$ are, respectively, the translational and the rotational friction constants of the sphere. The components, $H_{ij,\alpha\beta}^{TT}$, $H_{ij,\alpha\beta}^{RR}$, and $H_{ij,\alpha\beta}^{TR}$ only depend on the spatial arrangement of the spheres. In order to reduce the volume of computation, we neglect the presence of translational and rotational coupling motion by setting, $H_{ij,\alpha\beta}^{RT} = H_{ij,\alpha\beta}^{TR} = 0$. Indeed, in the calculation of diffusion constants for rigid molecules modeled as collections of spheres, Goldstein [16] and Wilson and Bloomfield [17] noted that the neglect of H_{ij}^{RT} and H_{ij}^{TR} is quite reasonable when the distance between the center of molecular rotation and a sphere in a rigid molecule, is much larger than the radius of the sphere. However, as noted by Dickinson, Allison and McCammon [18], translational and rotational coupling motion should be allowed for any calculation which attempts to treat translational mobilities at a level more precise than Oseen hydrodynamic.

We will now derive the explicit forms of the non-hydrodynamic forces included in the translational equation of motion. In the bead-spring model used in this study to represent a flexible fiber, the total non-hydrodynamic force in Eq. (8) is given by

$$\boldsymbol{F}_i^{nh} = \boldsymbol{f}_i^s + \boldsymbol{f}_i^b + \boldsymbol{f}_i^c, \tag{18}$$

where, $\boldsymbol{f}_i^s$, are the spring forces on the sphere i, $\boldsymbol{f}_i^b$ are the bending forces on this sphere and $\boldsymbol{f}_i^c$ are the total contact forces exerted on the sphere i by the adjacent spheres, i.e.,. $i-1$ and $i+1$.

The net spring forces, $\left\{\boldsymbol{f}_i^s\right\}_{i=2,N-1}$, exerted on each sphere to recover the equilibrium bonding distance are given by

$$\boldsymbol{f}_i^s = -k_s\left(\left|\boldsymbol{r}_i - \boldsymbol{r}_{i-1}\right| - 2a\right)\boldsymbol{t}_{i-1} + k_s\left(\left|\boldsymbol{r}_{i+1} - \boldsymbol{r}_i\right| - 2a\right)\boldsymbol{t}_i. \tag{19}$$

For the first and the last spheres, these forces are, respectively, given by

$$\boldsymbol{f}_1^s = k_s\left(|\boldsymbol{r}_2 - \boldsymbol{r}_1| - 2a\right)\boldsymbol{t}_1, \tag{20}$$

and

$$\boldsymbol{f}_N^s = -k_s\left(|\boldsymbol{r}_N - \boldsymbol{r}_{N-1}| - 2a\right)\boldsymbol{t}_{N-1}. \tag{21}$$

Here, k_s, is the stretching modulus or the spring constant. For an isotropic elastic cylinder with radius, a, the spring constant, k_s, is determined by the Young's modulus, E, as

$$k_s = \pi\, aE/2. \tag{22}$$

The bending forces can be derived as follows. Let θ_0 be the equilibrium bending angle. We consider a uniform fiber of homogeneous material subjected to only a moment at one end and an equal and opposite moment at the other end as shown in Fig. 3. Then the bending moments at each end, required to produce the change of curvature is given by

$$\boldsymbol{M}_{i+1}^b = k_b(\theta_i^b - \theta_0)\boldsymbol{b}_i, \tag{23}$$

$$\boldsymbol{M}_{i-1}^b = -k_b(\theta_i^b - \theta_0)\boldsymbol{b}_i. \tag{24}$$

Here, $\boldsymbol{b}_i$, is the unit vector normal to the bending plane, and is defined by,

$$\boldsymbol{b}_i = \frac{\boldsymbol{t}_{i-1} \times \boldsymbol{t}_i}{|\boldsymbol{t}_{i-1} \times \boldsymbol{t}_i|}, \tag{25}$$

while θ_i^b is the bending angle made by two adjacent bonds, defined by three adjacent spheres. Its value is estimated by taking the vector products of bonds connected the spheres, as

$$\cos\theta_i^b = \boldsymbol{t}_{i-1} \cdot \boldsymbol{t}_i. \tag{26}$$

Therefore, the bending restore forces acting on spheres, $i-1$, i, and $i+1$, are given by

$$\boldsymbol{f}_{i+1}^b = -\frac{1}{4a}\boldsymbol{M}_{i+1}^b \times \boldsymbol{t}_i, \tag{27}$$

$$\boldsymbol{f}_{i-1}^b = \frac{1}{4a}\boldsymbol{M}_{i-1}^b \times \boldsymbol{t}_{i-1}, \tag{28}$$

$$\boldsymbol{f}_i^b = -\left(\boldsymbol{f}_{i-1}^b + \boldsymbol{f}_{i+1}^b\right). \tag{29}$$

The bending constant, k_b, in Eqs. (23) and (24) is defined by the Young's modulus as

$$k_b = \pi a^3 E / 8 . \tag{30}$$

As far as the degradation or rupture of fibers is concerned, let, R_b, be the critical radius to break the fibers and $\theta_{b,crit}$ the corresponding critical bending angle. According to the thin rod theory, R_b, is given by

$$\frac{R_b}{a} = \frac{2}{\theta_{b,crit}} = \frac{E}{\sigma_b}, \tag{31}$$

where, σ_b is the ultimate tensile strength of the fiber. Hence, if the property, E/σ_b, is known, the calculated minimum value of the radius of curvature along the fiber, $R/a = 2/\theta_b$, at any stage of deformation can be used to predict the critical flow conditions to break the fibers.

Finally, the total contact force, $\boldsymbol{f}_i^c$, exerted on the sphere, i, is written as

$$\boldsymbol{f}_i^c = \boldsymbol{f}_{i,i-1}^c + \boldsymbol{f}_{i,i+1}^c, \tag{32}$$

where $\boldsymbol{f}_{i,i-1}^c$, and $\boldsymbol{f}_{i,i+1}^c$, are the contact forces exerted on the sphere, i, by the adjacent spheres, $i-1$, and $i+1$. The reaction forces the sphere, i, exerts on the adjacent spheres, $i-1$, and $i+1$ are $\boldsymbol{f}_{i-1,i}^c = -\boldsymbol{f}_{i,i-1}^c$ and $\boldsymbol{f}_{i+1,i}^c = -\boldsymbol{f}_{i,i+1}^c$, respectively.

As far as the rotational motion of the spheres is concerned, let's consider a pair of bonded spheres, $(i,i+1)$, and the local body coordinate system, $\{\boldsymbol{m}_i, \boldsymbol{n}_i, \boldsymbol{t}_i\}$, attached to that pair of bonded spheres. As described above, to compare the orientations of the fixed reference space coordinate system, $\{\boldsymbol{X}, \boldsymbol{Y}, \boldsymbol{Z}\}$, and the local body coordinate system, $\{\boldsymbol{m}_i, \boldsymbol{n}_i, \boldsymbol{t}_i\}$, the three Euler angles (ϕ, θ, ψ) are employed. If the reference space coordinate system is rotated through these three Euler angles, it will be brought into alignment with the body axes. For the rotational motion, the explicit forms of the torsional torques exerted on each sphere of the fiber model are obtained as follows. A pair of bonded spheres, $(i,i+1)$, may be subjected to a torsional torque and be twisted by an angle $\psi_{i,i+1} = \psi_{i+1} - \psi_i$, where, ψ_i, and ψ_{i+1}, are, respectively, the angular displacement of the spheres i and $i+1$ around the unit bond vector, $\boldsymbol{t}_i$. The angular displacement of the ith sphere, ψ_i, is given by Eq. (7), and depends on its angular velocity, $\boldsymbol{\omega}_i$. Then the following torques, $\{\boldsymbol{M}_i^t\}_{i=2,N-1}$, exert on each sphere to recover the equilibrium torsional angle, ψ_0,

$$\boldsymbol{M}_i^t = -k_t(\psi_{i-1,i} - \psi_0)\boldsymbol{t}_{i-1} + k_t(\psi_{i,i+1} - \psi_0)\boldsymbol{t}_i . \tag{33}$$

The torques exerted on the first and last spheres are given, respectively, by

$$\boldsymbol{M}_1^t = k_t(\psi_{1,2} - \psi_0)\boldsymbol{t}_1, \tag{34}$$

and

$$\boldsymbol{M}_N^t = -k_t(\psi_{N-1,N} - \psi_0)\boldsymbol{t}_{N-1}. \tag{35}$$

Here, the torsional torque constant, k_t, is defined by the shear modulus, G, as

$$k_t = \pi a^3 G/4. \tag{36}$$

Notice that, the rotational motion of spheres enters in the calculation of the torsional torques, Eqs. (33)-(35), through the torsional angles, $\{\psi_i\}_{i=1,N}$, given by Eq. (7).

A fiber may also break because it is twisted too sharply. According to the thin rod theory, the critical torsional angle, ψ_{crit}, to break the fibers by torsion is given by

$$\frac{2}{\psi_{crit}} = \frac{G}{\tau_t}, \tag{37}$$

where, τ_t, is the ultimate torsional shearing strength of the fiber. Hence, if the property, G/τ_t, is known, the calculated maximum value of the torsional angle, ψ, along the fiber, at any stage of deformation can be used to predict the critical flow conditions to break the fibers in any flow involving torsional deformation.

Finally, the total torque, $\boldsymbol{M}_i^c$, exerted on the sphere, i, by the contact forces on this sphere, is written as

$$\boldsymbol{M}_i^c = -a\,\boldsymbol{t}_{i-1} \times \boldsymbol{f}_{i,i-1}^c + a\,\boldsymbol{t}_i \times \boldsymbol{f}_{i,i+1}^c = a\,\boldsymbol{t}_{i-1} \times \boldsymbol{f}_{i-1,i}^c + a\,\boldsymbol{t}_i \times \boldsymbol{f}_{i,i+1}^c. \tag{38}$$

The resulting equations of motion including all forces and torques exert on each sphere then become

$$\boldsymbol{H}_{ij}^{TT} m_j \frac{d^2\boldsymbol{r}_j}{dt^2} + \left(\frac{d\boldsymbol{r}_i}{dt} - \boldsymbol{u}_0(\boldsymbol{r}_i)\right) = \boldsymbol{H}_{ij}^{TT}\left(\boldsymbol{f}_j^s + \boldsymbol{f}_j^b + \boldsymbol{f}_j^c\right), \tag{39}$$

$$\boldsymbol{H}_{ij}^{RR} I_j \frac{d^2\boldsymbol{\theta}_j}{dt^2} + \left(\frac{d\boldsymbol{\theta}_i}{dt} - \boldsymbol{\omega}_0(\boldsymbol{r}_i)\right) = \boldsymbol{H}_{ij}^{RR}\left(\boldsymbol{M}_j^t + \boldsymbol{M}_j^c\right). \tag{40}$$

To determine the contact forces between all paired spheres of the fiber model, $\{\boldsymbol{f}^c_{i,i+1}\}_{i=1,N-1}$, we take a view similar to that presented by Doi and Chen [19] to study the deformation and rupture of aggregating colloids in shear flows. We impose a condition that spheres can roll but not slip at their contact points. For, $i = 1, N-1$, this constraining condition is written as

$$\boldsymbol{u}_i + a\boldsymbol{\omega}_i \times \boldsymbol{t}_i = \boldsymbol{u}_{i+1} - a\boldsymbol{\omega}_{i+1} \times \boldsymbol{t}_i . \tag{41}$$

Differentiating Eq. (41), we have

$$\frac{d\boldsymbol{u}_i}{dt} + a\frac{d\boldsymbol{\omega}_i}{dt} \times \boldsymbol{t}_i + a\boldsymbol{\omega}_i \times \frac{d\boldsymbol{t}_i}{dt} = \frac{d\boldsymbol{u}_{i+1}}{dt} - a\frac{d\boldsymbol{\omega}_{i+1}}{dt} \times \boldsymbol{t}_i - a\boldsymbol{\omega}_{i+1} \times \frac{d\boldsymbol{t}_i}{dt} . \tag{42}$$

Calculating explicitly, $d\boldsymbol{t}_i / dt$, assuming, $d|\boldsymbol{r}_{i+1} - \boldsymbol{r}_i| / dt = 0$, (small extensibility of bonds compared to other forms of deformations), and substituting Eq. (41), we get the following equation

$$\begin{aligned} &\frac{d\boldsymbol{u}_i}{dt} + a\frac{d\boldsymbol{\omega}_i}{dt} \times \boldsymbol{t}_i + \frac{a}{|\boldsymbol{r}_{i+1} - \boldsymbol{r}_i|}\boldsymbol{\omega}_i \times (a\boldsymbol{\omega}_i \times \boldsymbol{t}_i + a\boldsymbol{\omega}_{i+1} \times \boldsymbol{t}_i) = \\ &\frac{d\boldsymbol{u}_{i+1}}{dt} - a\frac{d\boldsymbol{\omega}_{i+1}}{dt} \times \boldsymbol{t}_i - \frac{a}{|\boldsymbol{r}_{i+1} - \boldsymbol{r}_i|}\boldsymbol{\omega}_{i+1} \times (a\boldsymbol{\omega}_i \times \boldsymbol{t}_i + a\boldsymbol{\omega}_{i+1} \times \boldsymbol{t}_i) \end{aligned} . \tag{43}$$

The translational and rotational displacements of the N spheres defining the flexible fiber are obtained by the integration of Eqs. (39), (40) and (43).

In closing this section, it is worthwhile to stress again that, in the fiber model used here, spheres can roll but not slip at their contact points, to force the fiber, which consists of N rigid spheres, connected by $N-1$ bonds, to translate and rotate as whole body. Because of the continuity of a real fiber, we still consider the nonslip condition even if the fiber stretches, unless fracture occurs. This condition must be satisfied at each time step, between all paired spheres of the fiber model, without any numerical adjustment of the angles of the spheres. Finally, as far as very long fibers are concerned, the excluded volume interactions should be included, in order to prevent spheres or fiber from overlap. Addition of such interactions in the present model is straightforward. Here, since we are mainly interested in modeling the behavior of highly dilute fiber suspensions, of moderate aspect ratio, we do not explicitly include the excluded volume interactions in the model.

III. NUMERICAL RESULTS

To validate the fiber model developed in this study, we analyze in this section the motion of a fiber with aspect ratio, r_p, immersed in a Newtonian fluid with viscosity, η, whose

velocity field components are given by, $u = \dot{\gamma} y$, and $v = w = 0$, where $\dot{\gamma}$ is the steady shear rate, x and y coordinates are in the flow direction and the velocity gradient direction, respectively. For such a $2D$ simulation, the twisting deformation is negligible. We use the free draining approximation known for polymer dynamics. We consider the regime of low Reynolds number hydrodynamics, and neglect the inertia force of fluid and the spheres.

For a single ellipsoidal particle of aspect ratio, r_p, in simple shear flow, the analytical solution proposed by Jeffery, showed that the particle exhibits periodic motion through the same orbit, with a dimensionless orbit period of rotation, $T\dot{\gamma}$, that solely depends on r_p, as

$$T\dot{\gamma} = 2\pi\left(r_p + \frac{1}{r_p}\right). \tag{44}$$

A series of investigations by Trevelyan and Mason [14] and Bretherton [20] have shown that, the rotation of rigid rods of varying aspect ratios, at very low Reynolds numbers are in excellent agreement with the predictions of Eq. (44), provided that an equivalent ellipsoidal aspect ratio, r_e, calculated from the measured period of rotation, T, and Eq. (44), is used instead of r_p.

In Fig. 4 we compare the dimensionless orbit period of fiber rotation, $T\dot{\gamma}$, plotted as a function of aspect ratio, r_p, for a rigid ellipsoidal particle from Jeffery's theory with the experimental data of Trevelyan and Mason for rigid rods and predictions from the current model. Quantitative predictions of the model are impressive at moderate r_p. While the simulation results display correct trend, we observe a deviation of the predicted orbital period, $T\dot{\gamma}$, from the experimental data of Trevelyan and Mason around, $r_p = 50$. Such a deviation was also seen in the numerical results of Ross and Klingenberg. A more careful scrutiny of the experimental data provided by Trevelyan and Mason in Fig. 4 reveals that the measured $T\dot{\gamma}$ exhibits a change in the slope around, $r_p = 50$, in contradiction with Jeffery's theory for rigid ellipsoidal particles. According to that theory, the slope of $T\dot{\gamma}/2\pi$, for large values of r_p, remains constant with increasing r_p, and its value is about one, as can be seen from Eq. (44). Although Trevelyan and Mason reported that their experiments were carried out in the rigid rotation regime, a possible origin of such a change in the slope of the measured $T\dot{\gamma}$ around, $r_p = 50$, could be the onset of fiber buckling. In fact, Forgacs and Mason [21] derived a result for the onset of fiber bending by considering the axial stresses. They noted that for a given value of the relative strength of the flow, $\eta\dot{\gamma}/E$, there exists also a critical value of the aspect ratio of a fiber, $r_p = r_c$, at which the fiber will buckle. The solution corresponding to the first mode of buckling of the fiber is given by

$$\frac{\eta\dot{\gamma}}{E} = \frac{\ln 2r_c - 1.75}{2r_c^4}. \tag{45}$$

From Eq. (45), the relative strength of the flow to buckle a fiber with an aspect ratio of, $r_c = 100$, is around, $\eta\dot{\gamma}/E = 1.77\times10^{-8}$. Thus, when the apparent Young's modulus of the fiber is around, $E = 1\times10^{9}\ Nm^{-2}$, at a value of the flow strength of about $\eta\dot{\gamma} \approx 18\ Nm^{-2}$, the fiber will be bent, and the measured orbital period, $T\dot{\gamma}$, will deviate by changing the slope from that of a fully rigid cylindrical fiber of the same aspect ratio. Finally, the difference between the predicted $T\dot{\gamma}$ from that of Jeffery's theory is mainly attributed to the shape difference between ellipsoidal particles used in the Jeffery's theory and the current fibre model that uses a chain of spheres to mimic a cylindrical fiber. An equivalent ellipsoidal aspect ratio, r_e, calculated from the predicted period of rotation and Eq. (44), is used to take into account such a shape difference. Overall, the simulated results agree qualitatively with the experimental data and Jeffery's theory. This confirms the validity of the present model for a single rigid fiber.

We next consider the effect of fiber flexibility on the fiber rotation motion. The orbits of the ends of the fibers during a 360° rotation, with various bending coefficients k_b, in a simple shear flow are shown in Fig. 5. The fibers were initially aligned with the flow direction. It is clearly shown in Fig. 5 that the fiber deformation increases with decreasing the bending rigidity, k_b. The loci of the ends of the fibers are not symmetric about the y-axis. These results are supported by experimental data of Forgacs and Mason, who noticed that such a behavior is due to the compression forces (in the second and forth quadrants) and extension forces (in the first and third quadrants) experienced by single fibers during their rotational motion.

The fiber motions in simple shear flow over a wide range of the bending rigidity are shown in Figs. 6 and 7. The fiber was initially aligned in the x direction, and began to rotate in the flow gradient plane. The time sequences of orbits of fibers with aspect ratio, $r_p = 11$, are shown in Fig. 6. These results are in qualitative agreement with the experimental observation of Forgacs and Mason, who noted five regimes of motion: (a) Rigid motion, (b) S-turn, (c) snake turn, (d) springy rotation, and finally, coil formation shown in Fig. 7, where the fiber aspect ratio was increased to, $r_p = 31$. We recall that simulations with such an aspect ratio of, $r_p = 31$, may give unphysical results as the excluded volume interactions were not included in the model. To obtain the snake turn and the springy rotation, the fiber was initially given a small curvature, as shown in Fig. 6. Indeed, Forgacs and Mason also noted that the fiber deformed to an S-shape only when it was highly symmetrical, i.e., entirely free of any permanent deformations. In Fig. 7 that displays various stages of coil formation, it is clearly shown that, each end of the fiber moves independently of the other, in qualitative agreement with the experimental observation of Forgacs and Mason.

We now apply the model to predict critical flow conditions to break glass fibers, of known ultimate tensile strength, σ_b, and Young's modulus, E, as they rotate and deform in simple shear flow of a Newtonian fluid. The experimental study on breakage of glass fibers in simple shear was made by Salinas and Pittman [12]. In their work, the ultimate

value to break glass fibers, E/σ_b, was measured for two types of glass fibers. They noted that the breakage occurred when the radius of curvature along the fiber, R/a, falls to about 231. They also derived a correlation equation relating, R/a, $E/\eta\dot{\gamma}$, and r_p, that is only valid for fibers with $280 \le r_p \le 680$. Here, we wish to compare, qualitatively, the predicted trend of, R/a, with the experimental data reported by Salinas and Pittman for $11 \le r_p \le 25$, as the relative strength of the flow, $\eta\dot{\gamma}/E$, increases. In Fig. 8 we show the predicted minimum radius of curvature, R/a, which occurs at any point along the fiber at any stage of its rotation as a function of, $\eta\dot{\gamma}/E$, for various values of the aspect ratio, r_p. While the radius of curvature, R/a, decreases with increasing the flow strength, the rate at which R/a decreases is an increasing function of r_p, in qualitative agreement with the data reported by Salinas and Pittman. The flow strength, $\eta\dot{\gamma}/E$, necessary to reach a radius of curvature of about, $R/a = 200$, is increased by a factor of 10 as the aspect ratio, r_p, is reduced from 25 to 11. Considering that the critical radius of curvature at which breakage occurs is about 231, we show in Fig. 9 the critical relative strength of the flow, $\eta\dot{\gamma}/E$, to break glass fibers in simple shear flow as a function of the aspect ratio, r_p. The critical shear stress, $\eta\dot{\gamma}/E$, at which fibers broke exhibits an exponential decrease with increasing the aspect ratio, r_p. The overall trend is in qualitative agreement with the data of Salinas and Pittman, although the experimental data reported by them was for the range of fiber aspect ratio of $280 \le r_p \le 400$. These results show that the present model is able to correctly reproduce, at least qualitatively, the deformation and breakage conditions of single fibers, rotating in simple shear flow.

IV. CONCLUSIONS

A model for flexible fibers, consisting of a series of spheres, connected by stiff springs, that incorporates stretching, bending and twisting rigidities was proposed for direct simulation analysis of fiber deformation, and fiber breakage in simple shear flow. The effects of some parameters such as bending rigidity, fiber aspect ratio, and flow strength were discussed. The proposed model was validated. Overall, our numerical predictions are in qualitative agreement with experimental data provided in the literature. The current model also provides physical explanations about some mechanisms of fiber breakage. It is clear that there is no unique route to the fiber breakage process seen in flowing or processing of long fiber filled systems. Nevertheless, the present study suggests that, in any complex flow involving a combination of shear, torsional, and extensional flows, fiber breakage occurs when the minimum value of the ratio, $2/\theta_b$, or $2/\psi$, along the fiber, falls to below a prescribed critical value or when the maximum value of the ratio, $\left(\left|\boldsymbol{r}_i - \boldsymbol{r}_{i-1}\right| - 2a\right)/2a$, along the fiber exceeds a prescribed critical value, at any stage of deformation. These ratios depend on the shear stress, $\eta\dot{\gamma}$, the strain rate, $\dot{\varepsilon}$, the mechanical properties of fibers, E, and G, the fiber aspect ratio, r_p, along with the shape of the flow domain. Although the real picture is more complicated because a more complete description would also include interaction between fibers and the types of breakage, the above cited parameters are the key factors for the fiber degradation process.

References

[1]M. Doi and S.F. Edwards, *The theory of polymer dynamics*, (Oxford University Press, Oxford, 1986).
[2]S. Yamamoto and T. Matsuoka, J. Chem. Phys. **98**, 644 (1993).
[3]S. Yamamoto and T. Matsuoka, J. Chem. Phys. **100**, 3317 (1994).
[4]S. Yamamoto and T. Matsuoka, J. Chem. Phys. **102**, 2254 (1995).
[5]S. Yamamoto and T. Matsuoka, Polym. Eng. Sci. **35**, 1022 (1995).
[6]G.B. Jeffery, Proc. R. Soc. A **102**, 161 (1922).
[7]D. Qi, Int. J.Numer.Meth.Fluids **54**, 103 (2007).
[8]Z. Ning and J.R. Melrose, J. Chem. Phys. **111**, 10717 (1999).
[9]R.F. Ross and D.J. Klingenberg, J. Chem. Phys. **106**, 2949 (1997).
[10]P. Skjetne, R.F. Ross, and D.J. Klingenberg, J. Chem. Phys. **107**, 2108 (1997).
[11]S.B. Lindström and T. Uesaka, Phys. Fluid **19**, 113307 (2007).
[12]A. Salinas and J.F.T. Pittman, Polym. Eng. Sci. **21**, 23 (1981).
[13]B. Franzén, C. Klason, J. Kubat, and T. Kitano, Composites **20**, 65 (1989).
[14]B.J. Trevelyan and S.G. Mason, J. Colloid Sci. **6**, 354 (1951).
[15]P. Mazur and W. Van Saarloos, Physica **115A**, 21 (1982).
[16]R.F. Goldstein, J. Chem. Phys. **83**, 2390 (1985).
[17]R.W. Wilson and V.A. Bloomfield, Biopolymers **18**, 1205 (1979).
[18]E. Dickinson, S.A. Allison, and J.A. McCammon, J. Chem. Soc., Faraday Trans. 2 **81**, 591 (1985).
[19]M. Doi and D. Chen, J. Chem. Phys. **90**, 5271 (1989).
[20]F.P. Bretherton, J. Fluid Mech. **14**, 284 (1962).
[21]O.L. Forgacs and S.G. Mason, J. Colloid Sc. **14**, 473 (1959).

Captions for figures

Figure 1. Flexible fiber modeled as a series of N rigid spheres connected by stiff springs. (a) Configuration of a single fiber showing the bond vectors, $\boldsymbol{t}$, and the bending angle θ_b, and (b) two successive bonding spheres with the torsional angle $\psi_{i,i+1}$.

Figure 2. The fixed space coordinate system $\{\boldsymbol{X},\boldsymbol{Y},\boldsymbol{Z}\}$, the local body coordinate system, $\{\boldsymbol{m},\boldsymbol{n},\boldsymbol{t}\}$, and the line of nodes, N. The three Euler angles, (ϕ,θ,ψ), are defined by a sequence of three rotations. The first rotation is by an angle ϕ about the z-axis, the second is by an angle θ about the line node N, and the third rotation is by an angle ψ about the new t-axis. The resulting frame is $\{\boldsymbol{m},\boldsymbol{n},\boldsymbol{t}\}$.

Figure 3. Bending deformation made by two adjacent bonds defined by three adjacent spheres.

Figure 4. Dimensionless orbit period of rotation, $T\dot{\gamma}$, as a function of fiber aspect ratio, r_p, in simple shear flow. Comparison between Jeffery's theory for rigid ellipsoidal particles with experimental data of Trevelyan and Mason [14] for cylindrical fibers, and current model.

Figure 5. Polar plot of the loci of the ends of the fibers during rotation in simple shear flow, as the flexibility of the fiber is increased from $k_b = 10^2$ (rigid fiber) to $k_b = 10^{-3}$ (moderately flexible fiber).

Figure 6. Snapshots of rotational orbits of fibers with various flexibilities, in simple shear flow. (a) Rigid motion with $k_b = 10^2$, (b) S-turn with $k_b = 10^{-2}$, (c) snake turn with $k_b = 10^{-2}$, and (d) springy rotation with $k_b = 3\times10^{-2}$.

Figure 7. Snapshots of coil formation of a highly flexible fiber with $k_b = 10^{-5}$, in simple shear flow, at the different stages of coiling.

Figure 8. Minimum radius of curvature, R/a, which occurs at any point along the fiber at any stage of its rotation in simple shear flow.

Figure 9. Critical shear stress, $\eta\dot{\gamma}/E$, to break Pyrex glass fibers during flexible rotation in simple shear flow, as a function of the aspect ratio, r_p.

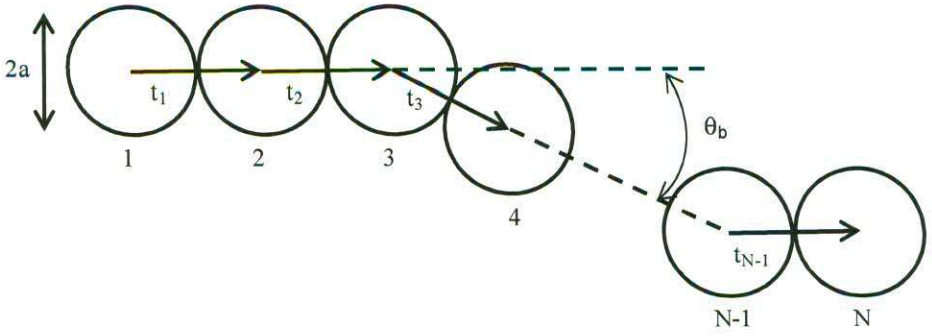

(a)

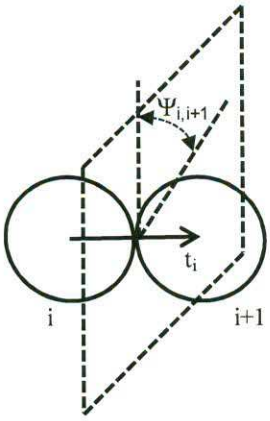

(b)

Figure 1. Flexible fiber modeled as a series of N rigid spheres connected by stiff springs. (a) Configuration of a single fiber showing the bond vectors, $\boldsymbol{t}$, and the bending angle θ_b, and (b) two successive bonding spheres with the torsional angle $\psi_{i,i+1}$.

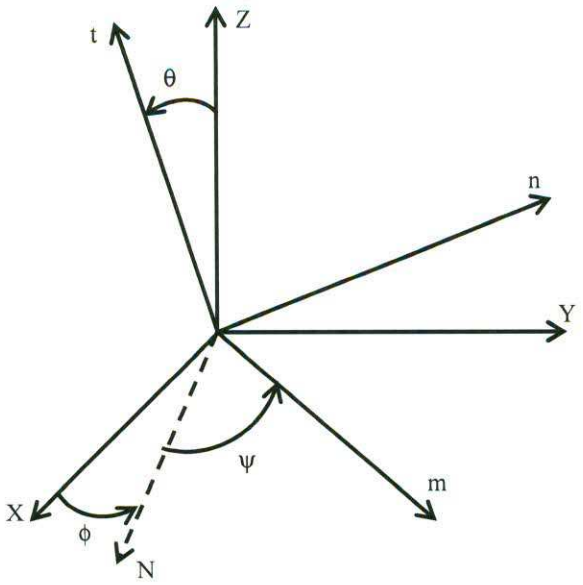

Figure 2. The fixed space coordinate system $\{\boldsymbol{X, Y, Z}\}$, the local body coordinate system, $\{\boldsymbol{m, n, t}\}$, and the line of nodes, N. The three Euler angles, (ϕ, θ, ψ), are defined by a sequence of three rotations. The first rotation is by an angle ϕ about the z-axis, the second is by an angle θ about the line node N, and the third rotation is by an angle ψ about the new t-axis. The resulting frame is $\{\boldsymbol{m, n, t}\}$.

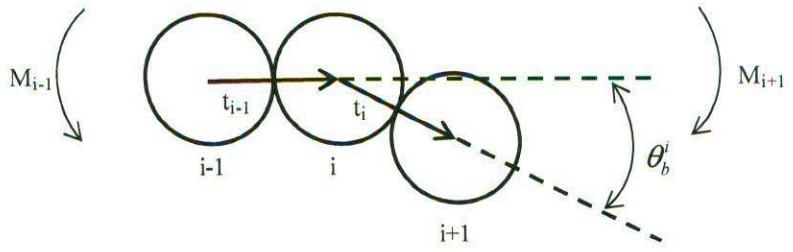

Figure 3. Bending deformation made by two adjacent bonds defined by three adjacent spheres.

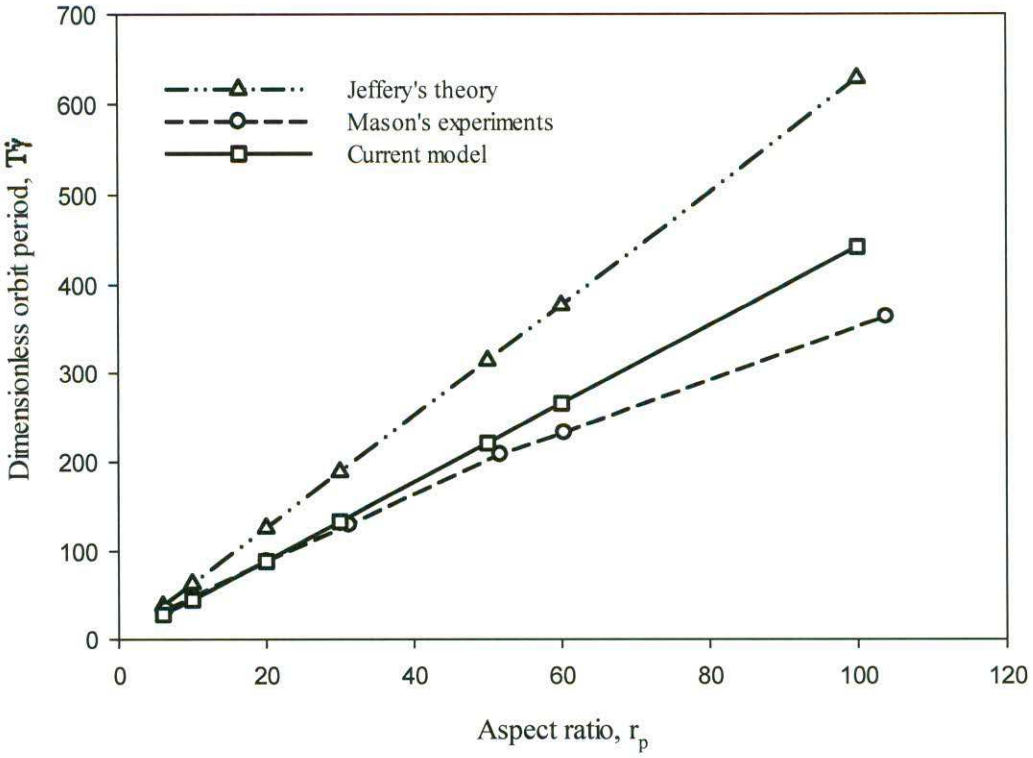

Figure 4. Dimensionless orbit period of rotation, $T\dot{\gamma}$, as a function of fiber aspect ratio, r_p, in simple shear flow. Comparison between Jeffery's theory for rigid ellipsoidal particles with experimental data of Trevelyan and Mason [14] for cylindrical fibers, and current model.

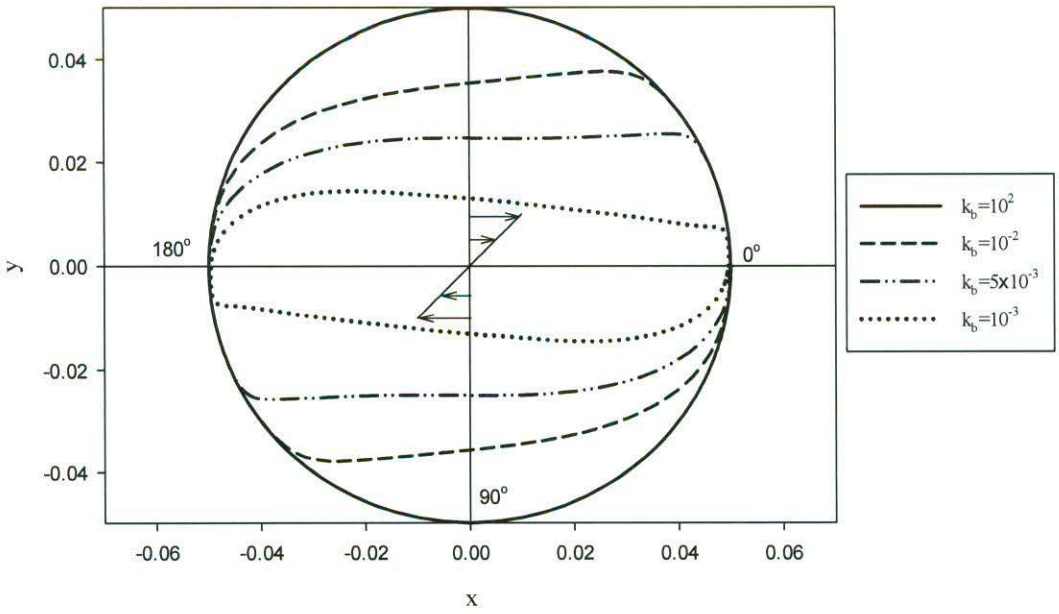

Figure 5. Polar plot of the loci of the ends of the fibers during rotation in simple shear flow, as the flexibility of the fiber is increased from $k_b = 10^2$ (rigid fiber) to $k_b = 10^{-3}$ (moderately flexible fiber).

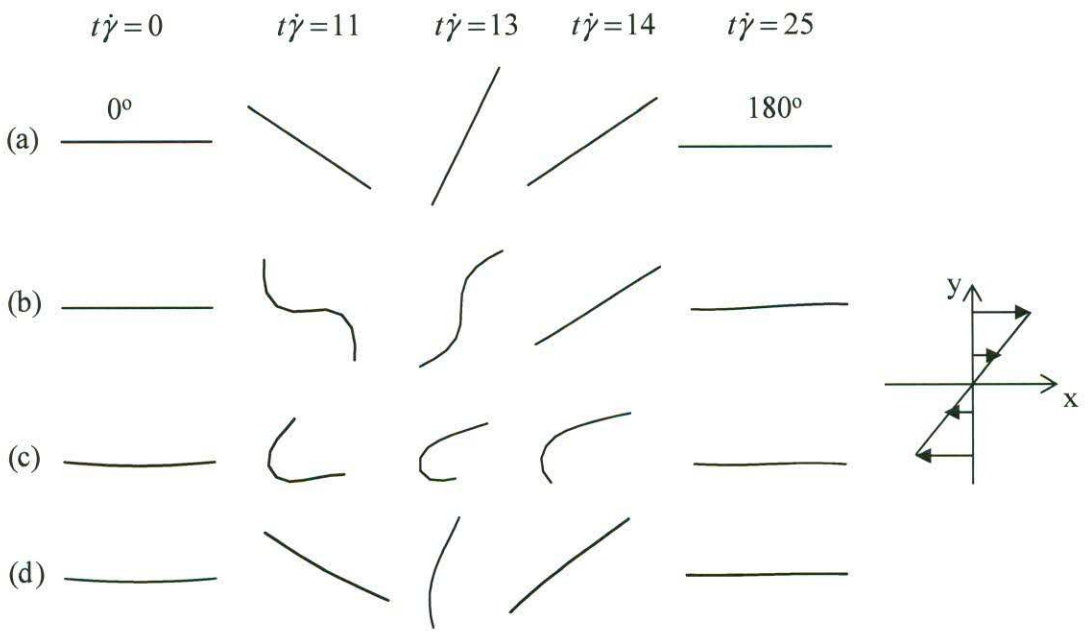

Figure 6. Snapshots of rotational orbits of fibers with various flexibilities, in simple shear flow. (a) Rigid motion with $k_b = 10^2$, (b) S-turn with $k_b = 10^{-2}$, (c) snake turn with $k_b = 10^{-2}$, and (d) springy rotation with $k_b = 3\times10^{-2}$.

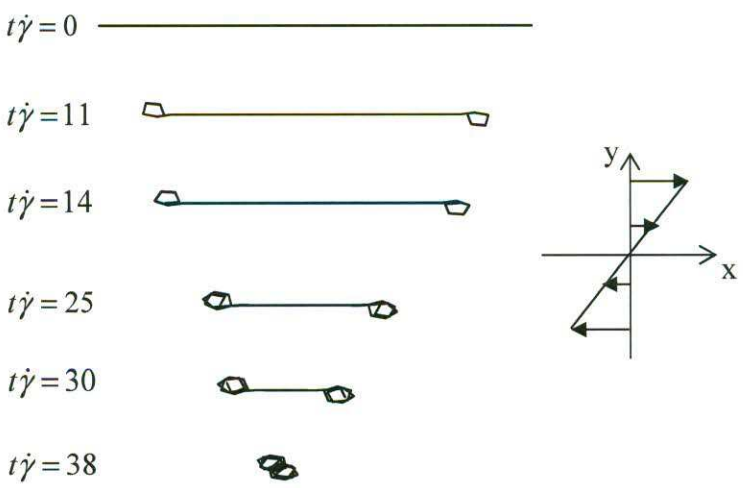

Figure 7. Snapshots of coil formation of a highly flexible fiber with $k_b = 10^{-5}$, in simple shear flow, at the different stages of coiling.

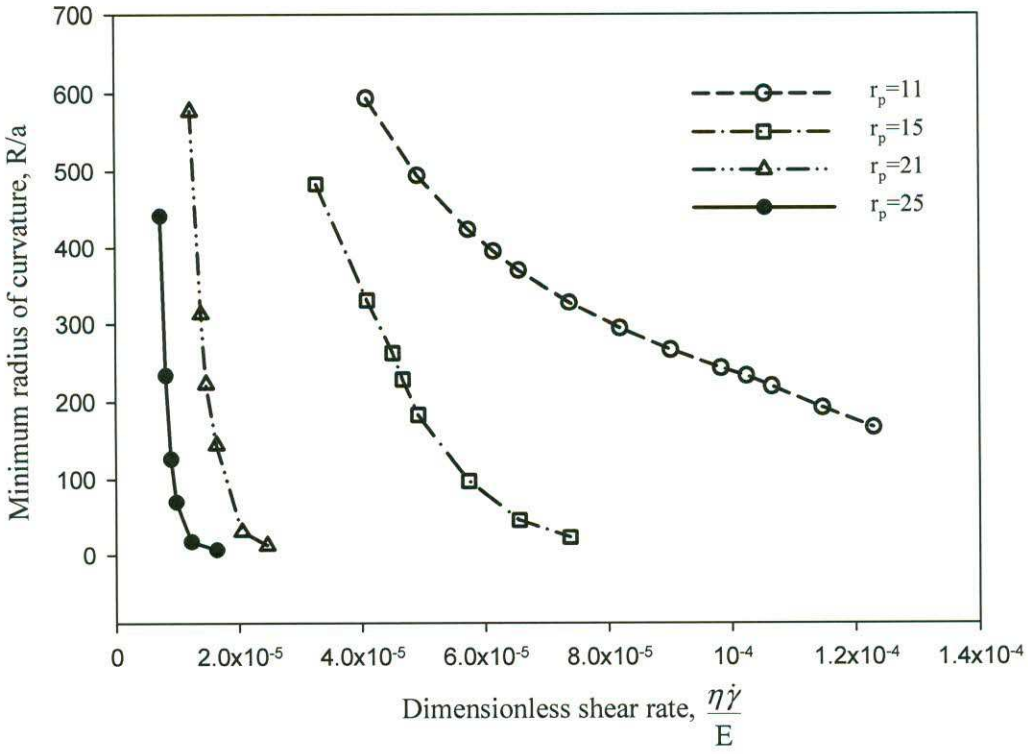

Figure 8. Minimum radius of curvature, *R/a*, which occurs at any point along the fiber at any stage of its rotation in simple shear flow.

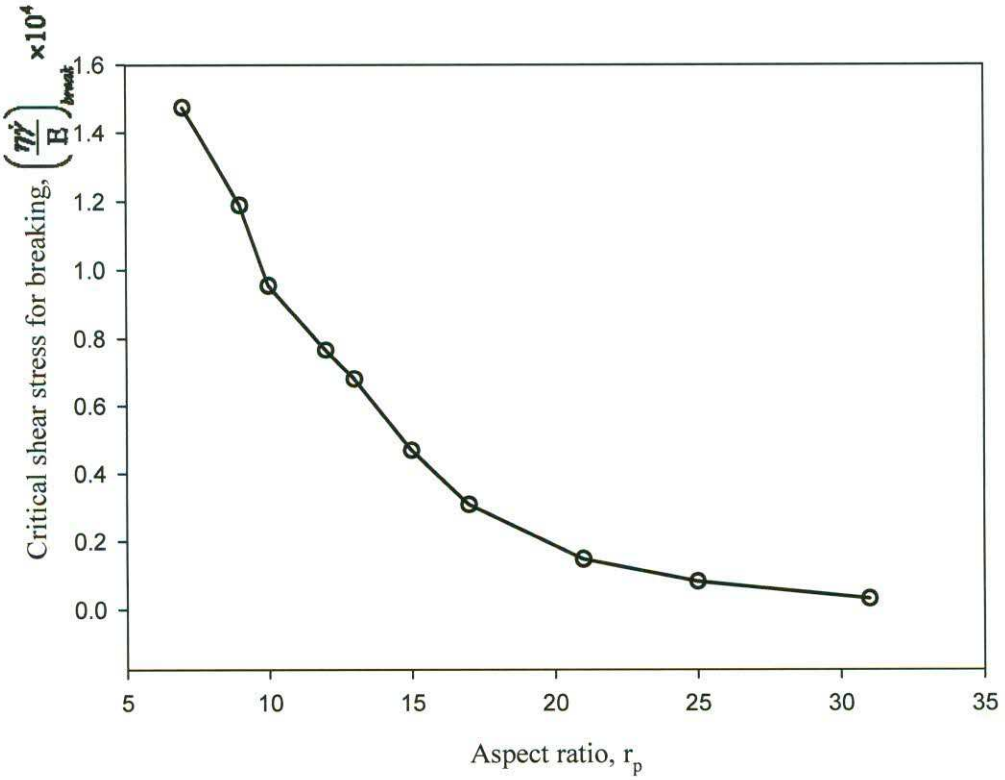

Figure 9. Critical shear stress, $\eta\dot{\gamma}/E$, to break Pyrex glass fibers during flexible rotation in simple shear flow, as a function of the aspect ratio, r_p.